AIAA JOURNAL
Vol. 47, No. 11, November 2009

Interface Conditions of Finite Difference Compact Schemes for Computational Aeroacoustics

Tomoaki Ikeda,* Takahiro Sumi,* and Takuji Kurotaki†
Japan Aerospace Exploration Agency, Tokyo 182-8522, Japan

DOI: 10.2514/1.42110

The interface condition provides flexibility to handle complex geometries on a set of structured grids. However, when used with a compact scheme to apply in computational aeroacoustics, its accuracy and stability may be degraded seriously by the boundary treatment that arises at a grid interface. To minimize this effect, a modified characteristic condition is incorporated in the finite difference compact scheme by using an explicit difference form at the boundary. The extension of this approach is naturally attained through the coordinate transformation of convective terms across an interface in multidimensions. The validity of current development is demonstrated through a simulation of trailing-edge noise generation from an airfoil at a low Mach number.

Nomenclature

$\boldsymbol{C}_\xi$	=	modified convection term in the ξ direction
c	=	convection velocity of a linear wave equation
$\boldsymbol{d}_\xi$	=	(x_ξ, y_ξ)
$\hat{\boldsymbol{E}}$	=	transformed inviscid flux in the ξ direction
$\boldsymbol{E}, \boldsymbol{F}$	=	inviscid fluxes in the x and y directions
h	=	width of a grid cell
Im()	=	imaginary part of a complex number
J	=	Jacobian matrix
k	=	wave number
L	=	one-dimensional domain length; the chord length of an airfoil
M	=	inflow Mach number
$\bar{P}^{-1}$	=	transformation matrix for characteristic decomposition
p_∞	=	ambient pressure
$\boldsymbol{R}$	=	characteristic differential variables
Re()	=	real part of a complex number
r	=	distance in the radial direction
$\boldsymbol{S}_\xi$	=	reduced source term of the characteristic relation in the ξ direction
U_∞	=	inflow velocity
u	=	one-dimensional function $u(x, t)$
$\hat{u}$	=	Fourier coefficient of u
u'	=	spatial derivative of u
u_o	=	initial condition of $u(x, t)$
δp_{rms}	=	rms value of pressure fluctuation
κ	=	modified wave number
λ	=	eigenvalue of the Gustafsson-Kreiss-Sundström stability analysis
$\bar{\lambda}$	=	diagonal matrix of the speeds of characteristics
ξ^L, η^L	=	generalized coordinate on the grid L
ξ^R, η^R	=	generalized coordinate on the grid R

I. Introduction

COMPACT finite difference schemes are now commonly used to achieve higher accuracy in many fields of computational analysis. Their low-dispersion nature is favored especially in the direct numerical simulations (DNS) or large-eddy simulations of turbulent flows, as well as aeroacoustics, to resolve short wavelengths with high accuracy. One of the advantages of finite difference schemes is that their formulations can be extended easily to general coordinates. Recently, many application studies have been done on generalized curved grids using upwind or centered compact schemes. Also, the attempts to solve more complicated geometries are being made through multiblock approaches [1,2]. Usually, in a multiblock framework, the numerical grids must be carefully constructed to smoothly bridge grid topologies at a block connection, because the abrupt variation lowers the accuracy of flow simulations. With increasing geometrical complexity, however, it would be inhibitive to meet this requirement. On the other hand, Kim and Lee [3] introduced the characteristic interface conditions that do not necessarily require the smooth connection at a block interface, where the characteristic relations are applied from both sides; this approach has been extended to a more general treatment which alleviates the local-axis dependence across an interface [4]. Alternatively, to handle a complex geometry on a structured-grid basis, an overset-grid technique allows the use of high-order schemes as well: an entire flow domain is subdivided into a set of smaller components with a possibly simpler configuration (e.g., [5,6]). However, the characteristic interface condition would also increase flexibility in discretizing a subdivided region, not only limited in a multiblock framework. The purpose of the present article is to clarify how these interface treatments affect the accuracy of compact schemes, especially when used in computational aeroacoustics (CAA).

One of the difficulties in interface conditions is the boundary treatment of compact schemes at the interface. Because the derivatives are expressed implicitly in compact schemes, even if formally high-order schemes are used for inner nodes, actual accuracy may degrade seriously, which would result in unstable modes by using inappropriate approximations. Many studies have been conducted for this issue. For instance, Carpenter et al. [7] performed the semi-discrete eigenvalue analysis, originally developed by Strikwerda [8], on high-order boundary schemes, and showed that increasing the accuracy of boundary conditions would lead to instability. From the view point of the Fourier analysis, Sengupta et al. [9] pointed out that the boundary implementation can be critical to the stability of compact schemes, by also applying the von Neumann analysis, and derived a family of optimized upwind compact schemes. Also, to achieve more accurate schemes, optimization techniques were introduced to boundary closures [10,11], combined with centered compact schemes.

In this paper, our aim is to construct a proper formulation of characteristic-based interface conditions for the use with compact schemes. Here, we primarily concern the implementation of centered finite difference compact schemes, which is suited to aeroacoustic problems on, for example, a low-Mach-number flow, as well as turbulent flow. To develop a proper interface condition, the boundary

Received 10 November 2008; revision received 23 June 2009; accepted for publication 24 July 2009.

*Research Associate, Fluid Dynamics Group.
†Senior Researcher, Fluid Dynamics Group. Senior Member AIAA.

closure of compact schemes will be first discussed using a Fourier mode analysis and tested through one-dimensional convection problems. Next, the extension to multidimensions will be presented. Finally, the developed interface condition is applied to a CAA test case, 2-D flow past an airfoil on the grid with singularity, and a resulting aerodynamic sound is quantitatively examined and discussed.

II. Analysis of the One-Dimensional Boundary Closure

A. Modified Wave Number Analysis

To evaluate the accuracy of finite difference schemes on phase space, it is common to use a Fourier mode analysis. When applying it to a compact scheme, however, the modified wave number of the scheme is not only a function of each mode, but also coupled spatially. A modified wave number is given as a form of implicit representation in an analytical expression; otherwise, in general, it must be solved with the dependence on the same modes at all other nodes, as shown in [9,10].

Here, we analyze a compact scheme applied to a convection problem for a function $u(x,t)$ defined over a bounded domain $x \in [0, L]$ at $t > 0$. After the homogeneous discretization of the domain by N nodes, or $N-1$ cells, the spatial derivative u' can be approximated by an implicit form

$$\sum_{l=j-n_L}^{j+n_R} a_{j,l} u'_l = \frac{1}{h} \sum_{l=j-m_L}^{j+m_R} b_{j,l} u_l \tag{1}$$

for $j = 1, 2, \ldots, N$, where n_L, n_R, m_L, and m_R represent the number of nodes required for the given stencils, h is the width of a cell, and $a_{j,l} = 1$ if $j = l$. For inner nodes, we usually apply uniform coefficients, namely, $a_{i,i+m} = a_{j,j+m}$ and $b_{i,i+m} = b_{j,j+m}$ for $i \neq j$. However, because the domain is bounded, we need to shift the stencils and therefore modify the coefficients near boundaries; this modification on a compact scheme is often referred to as a boundary compact scheme. Consequently, this also alters the behavior of modified wave numbers at all the locations. Because the spatial derivatives of a boundary scheme are usually coupled as those for inner nodes, its modified wave numbers are also coupled as a system of equations.

By applying discrete Fourier expansion, u_j can be written as

$$u_j = \sum_n \hat{u}_n e^{\mathrm{i}k_n h j}$$

where $\hat{u}_n$ is a Fourier coefficient of the nth mode, $k_n = 2\pi n/L$, and the summation on n is taken for a suitable range of N modes, for example, $-N/2$ to $N/2-1$ for an even number of N. Then, by definition, the Fourier coefficient of the approximated derivative term can be expressed by using the corresponding modified wave number $\kappa_n^{(j)}$ defined for the node j as $\mathrm{i}\kappa_n^{(j)} \hat{u}_n$. By substituting these relations into Eq. (1), we obtain an implicit representation of modified wave numbers for the nth Fourier mode,

$$\sum_l a_{j,l} \mathrm{i}\kappa_n^{(l)} e^{\mathrm{i}k_n h(l-j)} = \frac{1}{h} \sum_m b_{j,m} e^{\mathrm{i}k_n h(m-j)} \tag{2}$$

This can be solved using a conventional multidiagonal matrix inversion technique. However, because all the modified wave numbers are coupled, it would not be straightforward to derive effective coefficients for a boundary compact scheme, unlike the optimization for inner nodes by reducing a phase error (e.g., [12]). The optimized sets of boundary schemes in [3,11] were constructed without considering the aforementioned coupling. Therefore, their schemes show a considerable phase error near the boundary node, as shown in Fig. 1. On the other hand, in [10], optimized boundary schemes were obtained by calibrating free parameters included only in the boundary-node scheme to minimize phase error, whereas standard Padé schemes were used for inner nodes.

B. Test One-Dimensional Problem

As a test case of characteristic interface conditions, we consider a one-dimensional linear wave equation with convection velocity c (>0), imposing the periodic boundary condition. A one-dimensional periodic problem may be solved simply by only using an interior scheme with a common periodic inversion technique. However, because our objective is to examine the effect of boundary schemes when coupled with centered compact schemes, the periodicity here is enforced by a characteristic boundary condition applied to bounded schemes. Namely, we impose the continuity of the spatial derivative of a linear convection problem at both ends as

$$\frac{\partial u}{\partial t} + c\frac{\partial u}{\partial x} = 0, \qquad \left.\frac{\partial u}{\partial x}\right|_{x=0} = \left.\frac{\partial u}{\partial x}\right|_{x=L} \tag{3}$$

Because the convection velocity is positive, the derivative at $x = 0$ should be determined by that evaluated at $x = L$. Then, a bounded compact scheme given in Eq. (1) can be applied to this test case.

The preceding boundary implementation is one simple application of characteristic interface conditions for a one-dimensional scalar problem. For example, we may place the discontinuity of cell width across the periodic boundary by using a nonuniform grid, stretched gradually. Also on a curvilinear grid of multidimensions, the characteristic conditions can be effective to enforce periodicity, because the requirement of grid smoothness is removed across the periodic boundary.

In [3], the interface condition may reduce to one-dimension, originally developed for a three-dimensional case, as follows:

1) Evaluate the spatial derivative by a bounded compact scheme without specifying any boundary conditions.

2) Update the boundary nodes: the derivative at $x = 0$ is replaced by that evaluated at $x = L$.

Because the convective velocity c is positive, the positive $\mathrm{Im}(\kappa)$ acts as *antidiffusion* that may lead to numerical instability, as observed in Fig. 1 at relatively large k. However, the optimization process proposed in [10] also shows a difficulty in reducing a phase

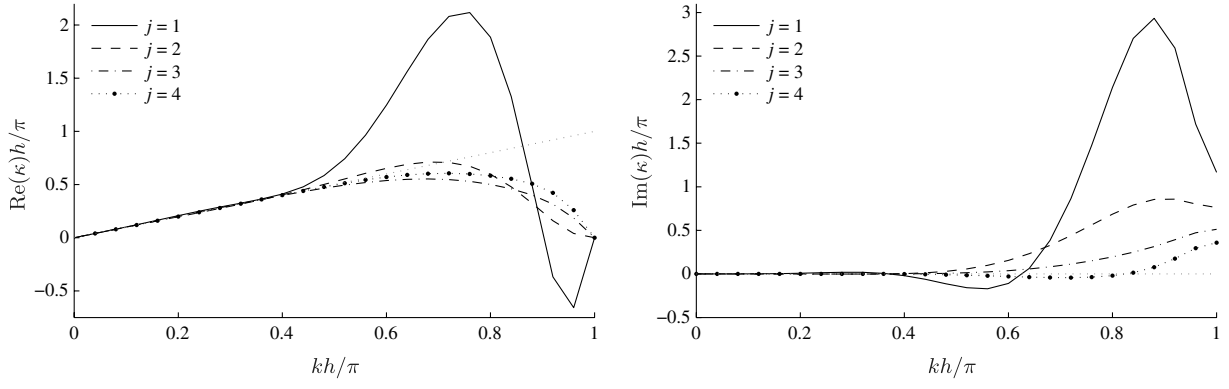

Fig. 1 Modified wave numbers for the scheme given in [3] near the left boundary. Total number of nodes N is 51. $\mathrm{Re}(\kappa)$ and $\mathrm{Im}(\kappa)$ denote the real and imaginary parts of a modified wave number, respectively.

error at the boundary node. The degradation of accuracy at boundary nodes can be critical when employed with characteristic interface or boundary conditions, especially in a multidimensional problem, for example, a vortex convected along an interface connection or acoustic disturbances reflected back and forth between two solid walls. To remove this difficulty, explicit stencils are used in [9] for the boundary and near-boundary nodes. Coupled with optimized upwind compact schemes, they attained stable implementations in terms of both modified wave numbers and von Neumann analysis.

By using an explicit scheme for the boundary node coupled with characteristic interface conditions, we can make a modification on the original implementation as follows:

1′) Evaluate the derivative at the upwind-side boundary node, $x = L$ in Eq. (3), by using an explicit difference scheme, which is employed as the boundary conditions to specify u'_1 and u'_N.

2′) Solve the system of equations of a compact scheme for the derivatives at inner nodes.

Here, we propose one test scheme to carry out the preceding modification. To demonstrate the validity of the present approach, we employ a set of standard finite difference schemes without any optimization. For the boundary nodes, $j = 1, N$, the standard third-order difference is adopted, whereas the standard Padé schemes are employed for the inner nodes: the fourth-order centered difference for the nodes adjacent to boundaries, and the sixth-order difference elsewhere. After enforcing the characteristic boundary condition, the finite difference form of the boundary scheme at $j = 1, 2, N-1$ and N is written as

$$u'_1 = u'_N = \frac{1}{6h}(11u_N - 18u_{N-1} + 9u_{N-2} - 2u_{N-3}) \tag{4}$$

$$\frac{1}{4}u'_{j-1} + u'_j + \frac{1}{4}u'_{j+1} = \frac{3}{4h}(u_{j+1} - u_{j-1}) \quad (j = 2, N-1) \tag{5}$$

Because the derivative at the boundary nodes is updated through an explicit scheme given by Eq. (4), the fourth-order Padé scheme Eq. (5) can be rewritten by eliminating u'_j at the boundary node. This leads to upwind-weighted stencils for both $j = 2$ and $N-1$, respectively, as follows:

$$u'_j + \frac{1}{4}u'_{j+1} = \frac{1}{h}\left[\frac{3}{4}u_{j+1} - \frac{29}{24}u_{j-1} + \frac{3}{4}u_{N-1} + \frac{3}{8}u_{N-2} + \frac{1}{12}u_{N-3}\right] \quad (j = 2) \tag{6}$$

$$u'_j + \frac{1}{4}u'_{j-1} = \frac{1}{h}\left[\frac{7}{24}u_{j+1} + \frac{3}{4}u_j - \frac{9}{8}u_{j-1} + \frac{1}{12}u_{j-2}\right] \quad (j = N-1) \tag{7}$$

In the following, the implement defined here is called the *present* scheme. The modified wave numbers near both boundaries are shown in Fig. 2. Although antidiffusion still arises in the middle to relatively large wave numbers, the scheme has shifted toward a more stable side by imposing the characteristic relation in a modified manner. The resolution in the phase space is relatively low, because standard schemes are employed with no optimization technique.

For comparison, we also test the compact representation for boundary nodes. The standard third-order one-sided compact difference is used instead of the explicit scheme, which is defined as

$$u'_j + 2u'_{j+1} = (u_j + 4u_{j-1} - 5u_{j-2})/2h \qquad (j = 1) \tag{8}$$

$$u'_j + 2u'_{j-1} = (5u_j - 4u_{j-1} - u_{j-2})/2h \qquad (j = N) \tag{9}$$

For the inner nodes, however, the same Padé schemes are employed as the present scheme. This combination of compact differences is used in other studies (e.g., [13]) and is also examined in [10]. The original interface implementation [3] is applied to this standard compact scheme, which is called the SC scheme here. Although the characteristic condition is imposed at $j = 1$, it does not affect the phase behavior of other near-boundary nodes, which results in antidiffusion in large k. Also, as the family of compact representations for the boundary scheme, the scheme given in [3] by Kim and Lee is referred to as the KL scheme, whereas the optimized scheme derived by Jordan [10] is defined as the J scheme in the following.

Finally, we would clarify the modification intended in the present scheme. If we apply the original characteristic interface implementation by Kim and Lee [3] to the standard set of finite differences

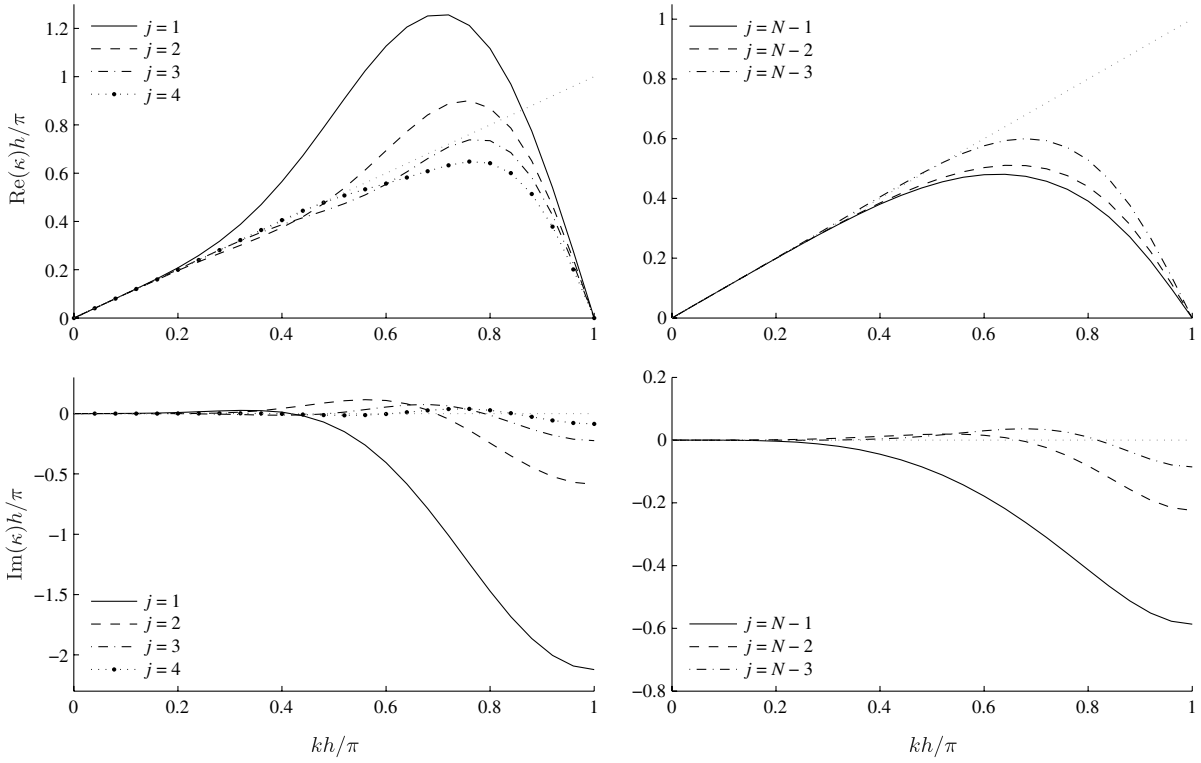

Fig. 2 Modified wave numbers for the present proposed scheme: (left) near the left boundary; (right) near the right boundary. Total number of nodes N is 51.

employed in the present scheme, the resultant finite difference form at $j = 2$ can be written as

$$u'_j + \frac{1}{4}u'_{j+1} = -\frac{1}{h}\left[\frac{7}{24}u_{j-1} + \frac{3}{4}u_j - \frac{9}{8}u_{j+1} + \frac{1}{12}u_{j+2}\right] \quad (j = 2) \tag{10}$$

Unlike Eq. (6), the stencils are weighted in the forward direction. The modified wave number profile at $j = 2$ is identical to the complex conjugate of that given at $j = N - 1$ in Fig. 2; therefore, it involves considerable antidiffusion in the middle to large k. Accordingly, this approach shows the behavior very similar to the SC scheme in the following linear test cases, although not presented.

C. Linear Convection Test

Here, four different schemes that use centered compact differences for inner nodes are examined via the linear convection problem, Eq. (3). In addition, an optimized upwind compact scheme, defined in [9] as OUCS-2, is also compared as a reference case; here, it is referred to as the OU scheme. Because the OU scheme employs explicit formulations for both the boundary and near-boundary nodes coupled with an interior scheme of five-point stencils, it does not lead to the difference as in Eqs. (6) and (10), depending on the implementation of characteristic conditions. As an initial condition, a periodic distribution is given as the form

$$u_o = \cos\left(\frac{2m\pi x}{L}\right)\exp\left[-C\left(x - \frac{L}{2}\right)^2\right] \tag{11}$$

In this test, $C = 25$, and $m = 3$ and 6 are employed. The total number of nodes N is 51, and the Courant–Friedrichs–Lewy number is chosen to be 0.2. Each scheme is advanced using the standard fourth-order Runge–Kutta scheme.

Figures 3 and 4 show the results after the run period of $20L/c$ and $5L/c$, respectively, for $m = 3$ and 6. In both cases, the J scheme given in [10] quickly diverged and is therefore not shown; the stability of the J scheme will be discussed in more detail in Sec. II.D by using an eigenvalue analysis. The KL scheme shows a considerable numerical diffusion, which can be predicted by the modified wave number distribution (Fig. 1). The boundary nodes have a fairly large dissipative error, which may add stability against the antidiffusion produced at near-boundary nodes. On the other hand, the SC scheme induced a spurious high-frequency noise added on the initial shape; it is specifically dominant in Fig. 4. Supposedly, u'_1, evaluated in Eq. (1) by the downwind difference, caused this instability through the implicit coupling of the compact scheme.

The present scheme of an interface implementation, however, agrees well with the exact solution, and the OU scheme also shows a reasonably accurate result with only a slight deviation, seen in Fig. 3, probably due to its lower-order boundary schemes. Both the schemes use noncompact explicit differences, which prefix a boundary condition of compact differences at boundary nodes. These observations

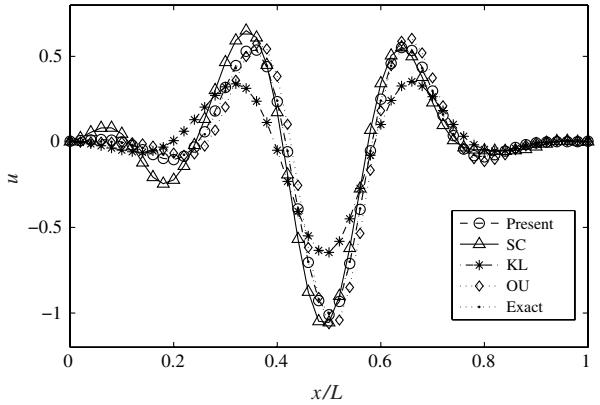

Fig. 3 One-dimensional test case after the run period of $20L/c$: $m = 3$ in Eq. (11).

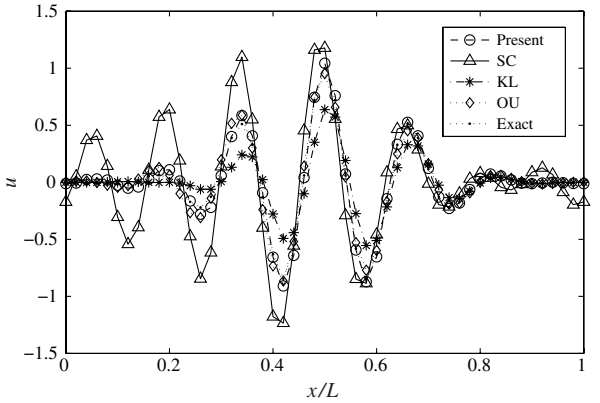

Fig. 4 One-dimensional test case after the run period of $5L/c$: $m = 6$ in Eq. (11).

indicate that the improper implementation of a boundary condition for compact schemes not only affects the stability, but can significantly lower the accuracy, which is critical to attain an accurate interface condition.

D. Semidiscrete Eigenvalue Analysis

This section briefly summarizes a stability criterion of linear convection, $\partial_t u + \partial_x u = 0$, using the eigenvalues of a semidiscrete system, namely, the Gustafsson-Kreiss-Sundström stability analysis (e.g., [7,8,12]). Here, we assume that the function $u(x, t)$ is discretized spatially with a uniform grid in $x \in [0, L]$, but still continuous in time. We apply a compact scheme to the spatial derivative as

$$A\boldsymbol{u}' = \frac{1}{h}B\boldsymbol{u} \tag{12}$$

where $\boldsymbol{u} = [u_i]$, $A = [a_{i,j}]$, and $B = [b_{i,j}]$ in Eq. (1). Then, its stability can be estimated through an eigenvalue problem $\lambda A\boldsymbol{u} = -B\boldsymbol{u}$. To fulfill a stability criterion, the real part of λ must be zero or negative. In fact, the distribution of eigenvalues λ can be affected greatly by the implementation of boundary conditions. Because the linear convection problem needs no boundary condition at the outlet $j = N$, we only require an inlet condition at $j = 1$. Here, we specify the spatial derivative u' at $j = 1$ as the boundary condition, instead of fixing $u(0, t) = u_1(t)$. When solving Eq. (12) for $\boldsymbol{u}'$, however, we assume that its right-hand side $\boldsymbol{u}$ is given, including u_1. We consider the following three types of boundary conditions (BCs):

BC-1: Explicitly prescribe u'_1 solving Eq. (12).

BC-2: Provide no boundary condition when solving Eq. (12). Afterward, replace u'_1 by the prescribed value.

BC-3: Impose the periodic boundary condition by a characteristic relation $u'_1 = u'_N$, as tested in the previous section.

BC-2 corresponds to the characteristic boundary conditions suggested by Kim and Lee [14]. Also, in [7], a stability analysis was performed based on the inflow boundary condition essentially equivalent to BC-2, whereas BC-1 was used in [12] as u'_1 set to zero.

In Fig. 5, the preceding three boundary conditions are compared by using the J scheme, and also the present scheme. On the J scheme, the diagram shows two distinct unstable eigenvalues in the right half of the plane for BC-2 and 3, although the scheme is stable for BC-1. The reason for the diverged solution by the J scheme in the linear convection test of Eq. (3) can be attributed to these unstable roots. On the other hand, when using the present scheme, both BC-1 and BC-2 are stable, whereas BC-3 shows slightly positive real eigenvalues. By imposing a characteristic-based periodic boundary condition, there exist several diffusive eigenvalues in the left half of the complex plane. However, the rest of the eigenvalues are aligned closely to the imaginary axis; some of them lie in the right half of the plane. This consequence is due to the enforcement of a periodic boundary condition, which indicates an infinite time integration using bounded schemes. If the linear convection test carried out in Sec. II.C is run for a considerably long period of time, these unstable modes may become apparent. In practice, to avoid the instability associated with

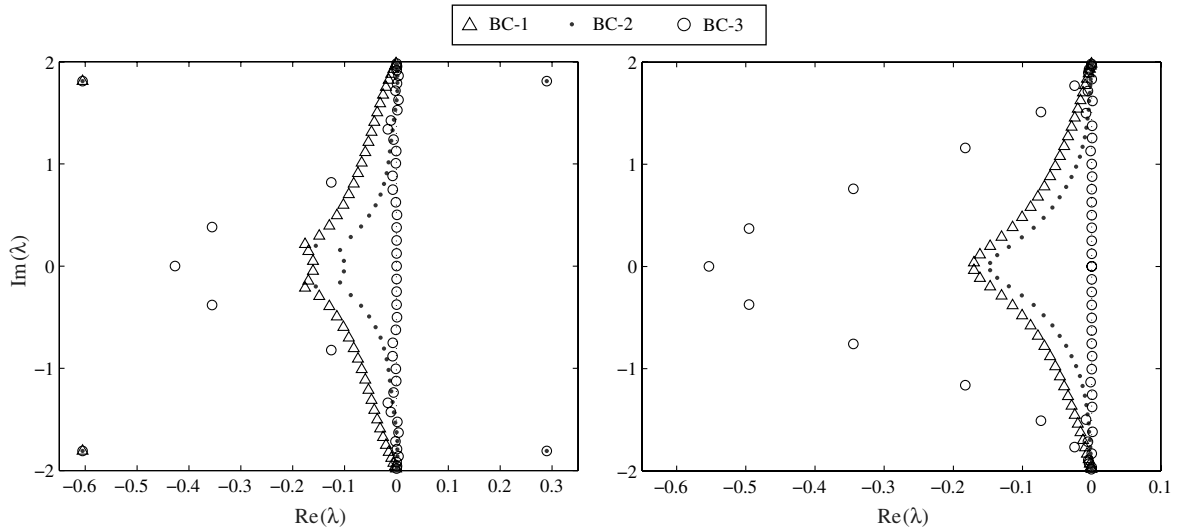

Fig. 5 Distributions of eigenvalues for three boundary conditions: (left) obtained by the J scheme; (right) the present scheme, respectively. Total number of nodes N is 51.

high-frequency errors, if any exist, the use of low-pass filters may be effective with a centered compact scheme, as also discussed in [15].

III. Formulation in Multidimensions

The interface condition proposed by [3] can be applied directly to a multidimensional problem. After convection terms are evaluated in all dimensions by a bounded compact scheme, their boundary values are updated via a quasi-linear one-dimensional characteristic relation, which can be written as

$$\frac{\partial \boldsymbol{R}}{\partial t} + \bar{\lambda}\frac{\partial \boldsymbol{R}}{\partial \xi} = \bar{P}^{-1}\boldsymbol{S}_\xi \tag{13}$$

where $\boldsymbol{R}$ represents the characteristic differential variables, $\bar{\lambda}$ is the diagonal matrix of the speeds of characteristics, $\bar{P}^{-1}$ is the transformation matrix for characteristic decomposition, and $\boldsymbol{S}_\xi$ denotes the reduced source term, including the convection terms, except the ξ direction, as well as the viscous terms. For simplicity, we only consider a two-dimensional case, and assume the ξ axis is the direction normal to the interface in computational coordinates. These assumptions are not requirements; we can easily extend the following discussion to a general three-dimensional problem. The decomposed convection term in the ξ direction is derived by multiplying $\bar{P}^{-1}$ from the left to

$$\boldsymbol{C}_\xi \equiv J\left[\frac{\partial \hat{\boldsymbol{E}}}{\partial \xi} - \left\{\boldsymbol{E}\frac{\partial}{\partial \xi}\left(\frac{\xi_x}{J}\right) + \boldsymbol{F}\frac{\partial}{\partial \xi}\left(\frac{\xi_y}{J}\right)\right\}\right] = \xi_x\frac{\partial \boldsymbol{E}}{\partial \xi} + \xi_y\frac{\partial \boldsymbol{F}}{\partial \xi} \tag{14}$$

so that $\bar{P}^{-1}\boldsymbol{C}_\xi = \bar{\lambda}\partial \boldsymbol{R}/\partial \xi$, where J is the transformation Jacobian, $\boldsymbol{E}$ and $\boldsymbol{F}$ are the inviscid fluxes in the x and y directions, respectively, and $\hat{\boldsymbol{E}} = (\xi_x \boldsymbol{E} + \xi_y \boldsymbol{F})/J$ is the transformed flux in the ξ direction.

However, when applying Eq. (13) to the present scheme to determine the boundary condition, the source term $\boldsymbol{S}_\xi$ must be precomputed carefully, because the convection terms that arise in $\boldsymbol{S}_\xi$ are generally unknown at this stage before solving a compact scheme. In the following, we would introduce an alternative treatment for multidimensions as an extension of the characteristic-based interface condition, without directly using the characteristic relation Eq. (13). Rather, a proper coordinate transformation is employed across an interface. A schematic of the general interface connection of two-dimensional grids is shown in Fig. 6.

When we would evaluate a ξ derivative on the grid R as a characteristic entering from the opposite side, grid L, the spatial derivatives should be estimated using the information on the grid L. This can be achieved via the following coordinate transformation from the grid R to L:

$$\frac{\partial}{\partial \xi^R} = x_{\xi^R}\frac{\partial}{\partial x} + y_{\xi^R}\frac{\partial}{\partial y} = x_{\xi^R}\left(\xi_x^L\frac{\partial}{\partial \xi^L} + \eta_x^L\frac{\partial}{\partial \eta^L}\right) + y_{\xi^R}\left(\xi_y^L\frac{\partial}{\partial \xi^L} + \eta_y^L\frac{\partial}{\partial \eta^L}\right) = (\boldsymbol{d}_{\xi^R}\cdot\boldsymbol{\nabla}\xi^L)\frac{\partial}{\partial \xi^L} + (\boldsymbol{d}_{\xi^R}\cdot\boldsymbol{\nabla}\eta^L)\frac{\partial}{\partial \eta^L} \tag{15}$$

where $\boldsymbol{d}_\xi = (x_\xi, y_\xi)$. The right-hand side of Eq. (15) can be understood as the directional derivative in the ξ^R direction evaluated on the grid L. The second term, the derivative in the tangential direction η^L, represents the discrepancy of the direction of ξ axis across an interface. The inner product $\boldsymbol{d}_{\xi^R}\cdot\boldsymbol{\nabla}\eta^L$ will be sufficiently small if two grids are connected smoothly. In finite difference form, the first term $\partial/\partial\xi^L$ is evaluated by the one-sided difference, whereas the second term $\partial/\partial\eta^L$ can be any high-order differences. In the following study, this tangential direction is evaluated by the same symmetric Padé scheme those used for inner nodes.

The implementation procedure of the proposed interface condition for a two-dimensional case can be summarized as follows:

1) On the boundary node of the grid R, compute the convection term in the ξ^R direction evaluated on its own grid $\boldsymbol{C}_{\xi^R}|_R$ as shown in Eq. (14).

2) Likewise, evaluate $\boldsymbol{C}_{\xi^R}$ on the opposite side, grid L, by applying the transformation shown in Eq. (15), denoted $\boldsymbol{C}_{\xi^R}|_L$.

3) Apply characteristic decomposition to both $\boldsymbol{C}_{\xi^R}|_R$ and $\boldsymbol{C}_{\xi^R}|_L$, and retain only the components of the upwind side for each

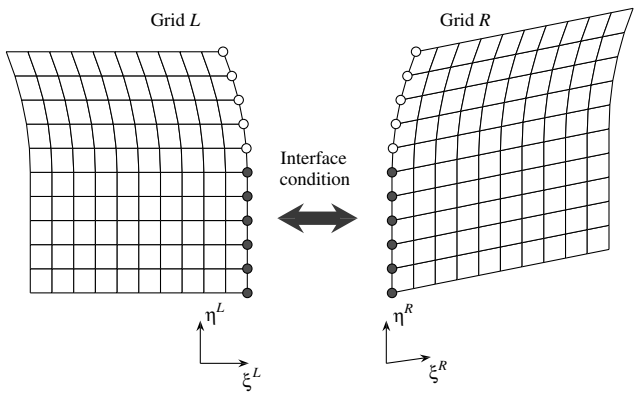

Fig. 6 Schematic of grids L and R, connected through an interface condition, applied to the nodes marked by filled circles. Open circles indicate other types of boundaries, for example, impermeable wall.

convection velocity. Combine them to reform $\boldsymbol{C}^*_{\xi^R}$. Then, reassess the convection term in the ξ^R direction through

$$\frac{\partial \hat{\boldsymbol{E}}^*}{\partial \xi^R} \equiv \frac{1}{J}\boldsymbol{C}^*_{\xi^R} + \left\{ \boldsymbol{E}\frac{\partial}{\partial \xi^R}\left(\frac{\xi^R_x}{J}\right) + \boldsymbol{F}\frac{\partial}{\partial \xi^R}\left(\frac{\xi^R_y}{J}\right)\right\} \tag{16}$$

4) On the boundary node of the grid L, follow the same process for $\boldsymbol{C}^{\xi_L}$.

5) Solve a compact scheme by using the resultant convection term for each grid as a boundary condition.

By taking these steps, because each side of the interface is evaluated in different numerical procedures, the physical variables will differ computed on each side. To ensure the continuity at the interface, they must be averaged in some way; here, we employ a simple arithmetic average.

We would note that the characteristic interface condition by Kim and Lee [3] requires the alignment of the gradient vectors of the coordinate normal to the interface, namely,

$$\nabla \xi^L / |\nabla \xi^L| = \nabla \xi^R / |\nabla \xi^R| \tag{17}$$

at the interface. The interface formulation derived in [16] also assumes a similar geometrical restriction. However, the approach presented here can relax this requirement. Geometrically, $\nabla\xi$ represents a vector normal to the surface of a constant ξ. Therefore, Eq. (17) is naturally satisfied when both entire boundary surfaces completely coincide. However, this does not hold on the interface shown in Fig. 6, as only a part of grid nodes match on the boundary, if the metrics are evaluated along boundary grid lines by using a compact scheme. In generalized coordinates, metrics should be computed by the finite difference form equivalent to that used in flow simulations [15]. If a part of boundary surfaces do not have a geometric correspondence with each other, where interface conditions would be omitted (e.g., the nodes marked by open circles in Fig. 6), the metrics evaluated there affect those at the interface, because a compact scheme generally has a global influence. Eventually, the normal vectors are not necessarily aligned across the interface when evaluated in finite difference forms, even if the local grid topologies are equivalent. The study by Sumi et al. [4] also discusses this issue and derives a generalized Jacobian-matrix representation in terms of quasi-linear characteristic relations for a multiblock interface. The present method can be extended to this type of grid as well; an application of this feature to a C-grid topology will be shown in Sec. IV.

On the other hand, if two interface surfaces match completely, the original formulation of characteristic interface conditions is still applicable. Instead of using the coordinate transformation shown in Eq. (15), $\boldsymbol{C}_{\xi^R}$ evaluated on the grid L can be expressed as

$$\boldsymbol{C}_{\xi^R}|_L = \boldsymbol{C}_{\xi^L}|_L - \boldsymbol{S}_{\xi^L} + \boldsymbol{S}_{\xi^R} \tag{18}$$

derived through the characteristic relation across the interface. In the original formulation, $\boldsymbol{S}_\xi$ contains the viscous terms, as well as the convection terms in the other directions. Because $\boldsymbol{C}_{\xi^R}$ is sought as the boundary condition of the convection term, we may exclude the viscous terms from $\boldsymbol{S}_\xi$; nevertheless, they also cancel out in an analytical form. In this case, we can show that Eq. (18) is analytically equivalent to the application of the coordinate transformation, Eq. (15), $\boldsymbol{C}_{\xi^R}$. Therefore, the method developed here reduces to an alternative representation of the characteristic interface condition.

IV. Sound Generation from a Two-Dimensional Airfoil

Finally, the present interface scheme is tested in an application problem of computational acoustics. In the flow past a two-dimensional object at a relatively low Reynolds number, it is well known that a dipole sound is generated accompanied with von Kármán vortex shedding. Direct simulations are able to reproduce this sound generation by using high-order numerical schemes. When constructing a numerical grid, however, great care must be taken not to affect the sound pressure that can be on the order of 10^{-4} or less [17].

As a verification test of the present methodology, we simulate the aerodynamic-noise generation from an NACA0012 airfoil using a C grid with the interface condition applied. The flow conditions are summarized as follows: the inflow Mach number $M = 0.2$; the Reynolds number $Re = U_\infty L/\nu = 5000$, where L is the chord length, ν is the kinematic viscosity at infinity; and the angle of attack is 5 deg. The fluid property is assumed to be of air; the specific-heat ratio is treated to be constant, 1.4. For the time advancement, the standard fourth-order Runge–Kutta scheme is used.

The numerical study in [18] also examined the noise generation from the foil using a sixth-order compact scheme. Nearly 2 million grid points were imposed on a C-grid topology to fully resolve the two-dimensional sound wave propagation up to $30L$ from the airfoil; a buffer layer was added to $500L$ to decay the outgoing sound waves and also the possible reflection at the outer boundaries. Their result is used as a reference case here. It should be noted that they needed to place a Cartesian grid in the wake region behind the trailing edge to remove a possible adverse effect on sound generation due to curved grid lines. In addition, the spatial derivative in the vertical direction was evaluated continuously in the Cartesian region to avoid the use of an interface, usually employed in C grid around an airfoil.

In our calculation, the numerical domain is limited to $30L$ in the radial direction and $50L$ in the downstream region, with a non-reflecting boundary condition applied to both the boundaries. Only a near- to middle-field is of interest for a quantitative comparison of sound levels to the reference case. Therefore, the number of grid points is rather small: $900 \times 250 = 0.23$ million. We also conducted a grid-convergence study to confirm that the near-field velocity and pressure fluctuations do not greatly vary by increasing the grid resolution, although the far-field pressure level does show the adverse effects of the present coarse grid, typically for $r > 10L$, where r is the radial distance from the airfoil. The numerical grid is shown in Fig. 7. The airfoil is tilted by 5 deg to the streamwise direction; the trailing edge of the airfoil is located at the origin. The interface condition is applied along with the grid line extended from the trailing edge toward the wake region. As seen from the figure, no efforts were made to smooth the grid near the interface connection. Rather, the grid holds the singular slope variation. Because the generated von Kármán vortices are supposed to convect along with the interface line, an ill-formed interface condition would easily create a fictitious pressure disturbance from the connection.

Figure 8 shows the instantaneous pressure fluctuation after the von Kármán vortex has fully developed in the wake. The obtained frequency of vortex shedding is 1.8, normalized by U_∞/L, which agrees with that reported in the reference case [18]. Generally, the pressure field is more prone to receive numerical errors, because its fluctuation normalized with the ambient pressure is very small.

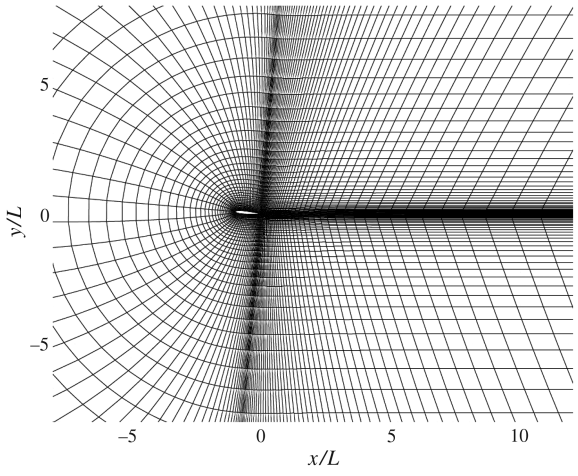

Fig. 7 C-grid topology around the airfoil. Grid lines are coarsened by a factor of 5 for visualization.

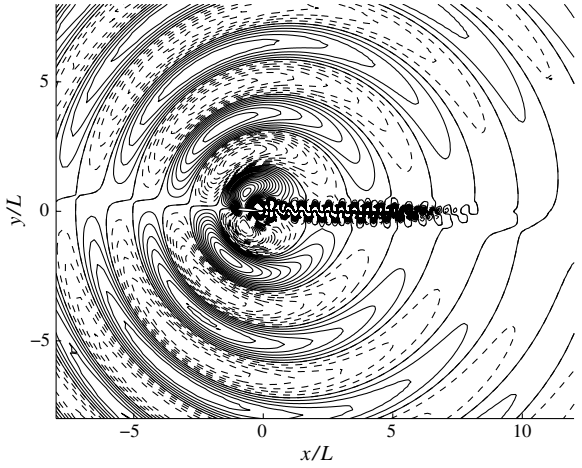

Fig. 8 Instantaneous pressure fluctuation δ_p. One contour level denotes $2.0 \times 10^{-5} p_\infty$. Solid and dashed lines denote positive and negative values, respectively.

However, these pressure visualizations clearly capture the propagation of a dipole sound generated at the airfoil. No spurious pressure fluctuation is recognized at the interface connection, where the vortex street coexists. This can be confirmed by the closer view of Fig. 9; synchronizing with the vortex shedding, aerodynamic sound is scattered from the trailing edge. The obtained sound pressure field here is also consistent with that shown in [18].

To quantitatively examine the obtained sound pressure, the root-mean-square values of pressure fluctuation δp_{rms} are plotted in Fig. 10 on the radial distance vertically upward from the middle of the airfoil. The amplitude of a dipole sound shows the dependence on $r^{-1/2}$ [17]; it is also shown in the figure. By comparing the present result to the reference case [18], although a slight discrepancy can be seen relatively near the foil, these two results agree quite well, in spite of the difference in the grid resolution. The result is presented up to $r = 15L$. Beyond that, δp_{rms} obtained in the present calculation starts to deviate from the $r^{-1/2}$ dependence due to the insufficient resolution. Nevertheless, this comparison provides an adequate validation for the present numerical treatment, in conjunction with the qualitative behavior of a dipole sound generation observed in Fig. 8.

The far-field sound pressure is approximated by using the time-harmonic force acting on the airfoil in polar coordinates [19]:

$$\delta p_{\mathrm{rms}}(r,\theta) = \frac{\rho_\infty c_\infty^2}{4}\left[\frac{M^5 St}{r/L}\left(C_l|_{\mathrm{rms}}\sin\theta + C_d|_{\mathrm{rms}}\cos\theta\right)^2\right]^{1/2} \quad (19)$$

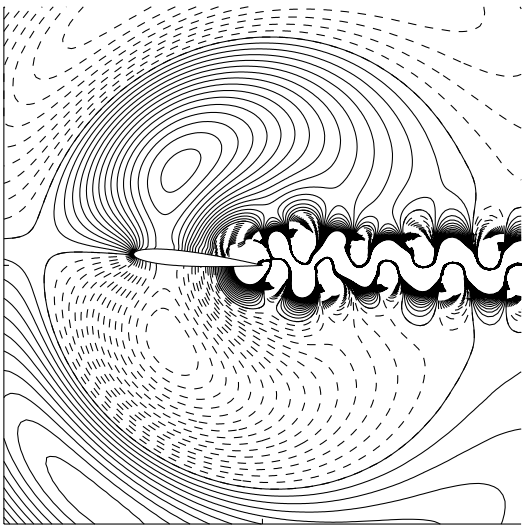

Fig. 9 Close view of instantaneous pressure fluctuation around the airfoil (see also caption of Fig. 8).

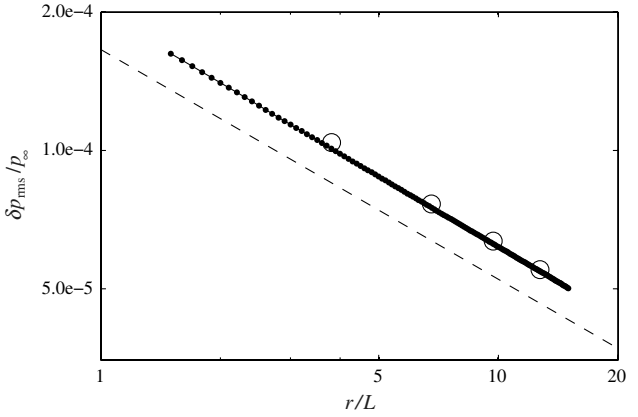

Fig. 10 Decay of pressure fluctuation: filled circle denotes present result; open circle denotes reference case [18]; dashed line denotes $r^{-1/2}$ dependence for reference.

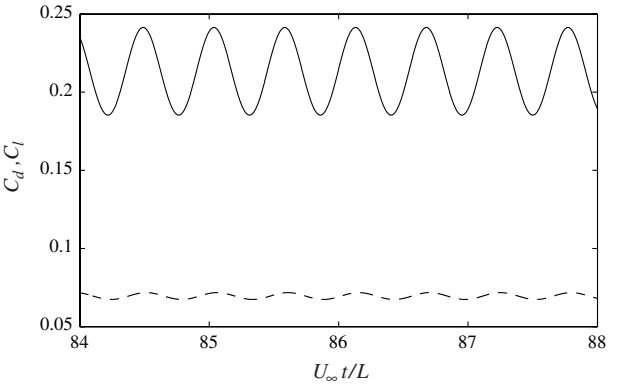

Fig. 11 Time history of drag and lift coefficients.

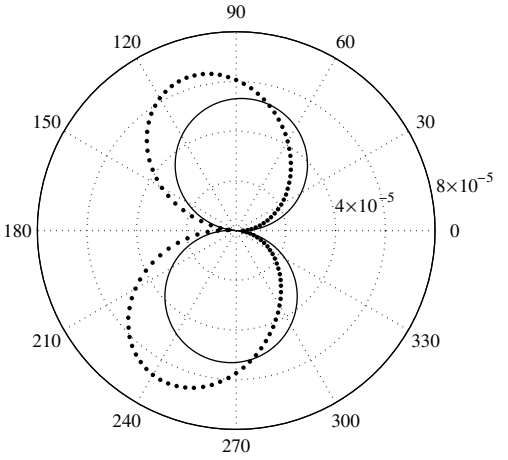

Fig. 12 Polar diagram of $\delta p_{\mathrm{rms}}/p_\infty$ at $r = 10L$: filled circle denotes present result; solid line denotes analytical estimation of low-frequency limit.

where St is the normalized shedding frequency 1.8, and C_l and C_d are the time-dependent lift and drag coefficients, respectively. The time-harmonic behavior of C_l and C_d is shown in Fig. 11. The estimation of Eq. (19) is valid in the low-frequency limit, where the two-dimensional airfoil is regarded to be acoustically compact. In the present calculation, one acoustic wavelength λ is estimated as $2.8L$, which may be slightly too small to apply the low-frequency approximation. Figure 12 shows the polar diagram of $\delta p_{\mathrm{rms}}/p_\infty$ at $r = 10L$. Although the low-frequency estimation of Eq. (19) indicates a simple dipole distribution, the present result shows a rather skewed profile in the upstream direction. However, it is very

similar to the case of $\lambda = 2L$ in the numerical work by Oberai et al. [20]; in their computation, the sound scattering effect on the airfoil surface is rigorously considered by solving Lighthill's equation for an artificial sound source placed near the trailing edge. Therefore, this is the consequence of sound generation from the flow around a noncompact airfoil. The deviation from the ideal dipole distribution given by Eq. (19) would be more evident as the wavelength decreases compared to the chord length.

V. Conclusions

We presented an interface condition using finite difference compact schemes suited to CAA problems. The modified wave number analysis indicates that the original approach by Kim and Lee [3] exhibits a considerable antidiffusion effect that lowers the stability. In addition, the boundary closure of existing compact schemes often lowers the accuracy in Fourier space as well. To regain the stability near an interface, the convection term evaluated on the upwind side of the interface should be applied to a compact scheme as its boundary condition. By using an explicit finite difference form at boundary nodes, this modification is achieved naturally. A combination of standard difference forms was employed as a model scheme to implement the present interface condition. The validity of this modified approach was also confirmed through a posteriori studies in terms of both stability and accuracy.

The extension of the interface condition to a general multidimension case is attained through the transformation on the local grid coordinates across an interface. As a two-dimensional CAA test case, the flow past a two-dimensional airfoil was simulated on a C-grid topology. In spite of the grid singularity placed in the wake region, the present scheme successfully reproduced the von Kármán vortex shedding and the associated aerodynamic-noise generation from the airfoil. The quantitative agreement with an available DNS study also supports the validity of our methodology; this approach minimizes the spurious sound generation at the interface connection without taking great care in mesh smoothing. This will allow the accessible use of high-order schemes to more complicated geometries, especially in three-dimensional problems.

Acknowledgments

The authors gratefully acknowledge the direct numerical simulation data and helpful comments provided by Tomohiro Irie at Tohoku University (currently Software Cradle Company, Ltd.).

References

[1] Visbal, M. R., and Gaitonde, D. V., "Padé-Type Higher-Order Boundary Filters for the Navier–Stokes Equations," *AIAA Journal*, Vol. 38, No. 11, 2000, pp. 2103–2112. doi:10.2514/2.872

[2] Imamura, T., Enomoto, S., Yokokawa, Y., and Yamamoto, K., "Simulation of the Broadband Noise from a Slat Using Zonal LES/RANS Hybrid Method," AIAA Paper 2007-226, 2007.

[3] Kim, J. W., and Lee, D. J., "Characteristic Interface Conditions for Multiblock High-Order Computation on Singular Structured Grid," *AIAA Journal*, Vol. 41, No. 12, 2003, pp. 2341–2348. doi:10.2514/2.6858

[4] Sumi, T., Kurotaki, T., and Hiyama, J., "Generalized Characteristic Interface Conditions for High-Order Multi-Block Computation," *International Journal of Computational Fluid Dynamics*, Vol. 21, No. 9, 2007, pp. 335–350. doi:10.1080/10618560701721736

[5] Delfs, J. W., "An Overlapped Grid Technique for High Resolution CAA Schemes for Complex Geometries," AIAA Paper 2001-2199, 2001.

[6] Sherer, S. E., and Scott, J. N., "High-Order Compact Finite Difference Methods on General Overset Grids," *Journal of Computational Physics*, Vol. 210, No. 2, 2005, pp. 459–496. doi:10.1016/j.jcp.2005.04.017

[7] Carpenter, M. H., Gottlieb, D., and Abarbanel, S., "The Stability of Numerical Boundary Treatments for Compact High-Order Finite Difference Schemes," *Journal of Computational Physics*, Vol. 108, No. 2, 1993, pp. 272–295. doi:10.1006/jcph.1993.1182

[8] Strikwerda, J. C., "Initial Boundary Value Problems for the Method of Lines," *Journal of Computational Physics*, Vol. 34, No. 1, 1980, pp. 94–107. doi:10.1016/0021-9991(80)90114-X

[9] Sengupta, T. K., Ganeriwal, G., and De, S., "Analysis of Central and Upwind Compact Schemes," *Journal of Computational Physics*, Vol. 192, No. 2, 2003, pp. 677–694. doi:10.1016/j.jcp.2003.07.015

[10] Jordan, S. A., "The Spatial Resolution Properties of Composite Compact Finite Differencing," *Journal of Computational Physics*, Vol. 221, No. 2, 2007, pp. 558–576. doi:10.1016/j.jcp.2006.06.026

[11] Kim, J. W., "Optimised Boundary Compact Finite Difference Schemes for Computational Aeroacoustics," *Journal of Computational Physics*, Vol. 225, No. 1, 2007, pp. 995–1019. doi:10.1016/j.jcp.2007.01.008

[12] Lele, S. K., "Compact Finite Difference Schemes with Spectral-Like Resolution," *Journal of Computational Physics*, Vol. 103, No. 1, 1992, pp. 16–42. doi:10.1016/0021-9991(92)90324-R

[13] Suh, J., Frankel, S. H., Mongeau, L., and Plesniak, M. W., "Compressible Large Eddy Simulations of Wallbounded Turbulent Flows Using a Semi-Implicit Numerical Scheme for Low Mach Number Aeroacoustics," *Journal of Computational Physics*, Vol. 215, No. 2, 2006, pp. 526–551. doi:10.1016/j.jcp.2005.10.036

[14] Kim, J. W., and Lee, D. J., "Generalized Characteristic Boundary Conditions for Computational Aeroacoustics," *AIAA Journal*, Vol. 38, No. 11, 2000, pp. 2040–2049. doi:10.2514/2.891

[15] Visbal, M. R., and Gaitonde, D. V., "On the Use of Higher-Order Finite Difference Schemes on Curvilinear and Deforming Meshes," *Journal of Computational Physics*, Vol. 181, No. 1, 2002, pp. 155–185. doi:10.1006/jcph.2002.7117

[16] Nordström, J., and Carpenter, M. H., "High-Order Finite Difference Methods, Multidimensional Linear Problems, and Curvilinear Coordinates," *Journal of Computational Physics*, Vol. 173, No. 1, 2001, pp. 149–174. doi:10.1006/jcph.2001.6864

[17] Inoue, O., and Hatakeyama, N., "Sound Generation by a Two-Dimensional Circular Cylinder in a Uniform Flow," *Journal of Fluid Mechanics*, Vol. 471, Nov. 2002, pp. 285–314.

[18] Irie, T., Hatakeyama, N., and Inoue, O., "Direct Numerical Simulation of Aerodynamic Noise Around an Airfoil," *Proceedings Eighth Japan-Russia Joint Symposium on Computational Fluid Dynamics*, Japan Society of Fluid Mechanics, Tokyo, 2003, pp. 14–15.

[19] Blake, W. K., *Mechanics of Flow-Induced Sound and Vibration*, Vol. 1, Academic Press, New York, 1986.

[20] Oberai, A. A., Roknaldin, F., and Hughes, T. J. R., "Computation of Trailing-Edge Noise Due to Turbulent Flow over an Airfoil," *AIAA Journal*, Vol. 40, No. 11, 2002, pp. 2206–2216. doi:10.2514/2.1582

C. Bailly
Associate Editor